Cover Page

1) Title of the paper:

Chromatic and wavefront aberrations: L-, M- and S-cone stimulation with typical and extreme retinal image quality

2) authors' affiliation and address:

*** Psychology, University of Chicago, 940 E. 57th Street, Chicago, IL 60637, USA**

*** Ophthalmology & Visual Science and Institute for Mind & Biology, University of Chicago, 940 E. 57th Street, Chicago, IL 60637, USA**

*** Ecole Polytechnique de l'Université de Nantes, IRCCyN, Rue Ch. Pauc, La Chantrerie, BP 50609, 44306 Nantes Cedex 03, France**

*** School of Optometry, Indiana University, 800 E. Atwater Avenue, Bloomington, IN 47405, USA**

3) e_mail address:

Florent.Autrusseau@univ-nantes.fr

4) Journal & Publisher information:

Elsevier

http://www.journals.elsevier.com/vision-research/

5) bibtex entry:

```
@ARTICLE{VisionResearch2011,
  author = {F. Autrusseau and L. Thibos and S.K. Shevell},
  title = {Chromatic and Wavefront Aberrations: L-, M- and S-cone Stimulation
          with Typical and Extreme Retinal Image Quality},
  journal = {Elsevier Vision Research},
  year = {2011},
  volume = {51},
  pages = {21-22}
}
```

doi: http://dx.doi.org/10.1016/j.visres.2011.08.020

Vision Research 51 (2011) 2282–2294

Contents lists available at SciVerse ScienceDirect

Vision Research

journal homepage: www.elsevier.com/locate/visres

Chromatic and wavefront aberrations: L-, M- and S-cone stimulation with typical and extreme retinal image quality

Florent Autrusseau [a,c], Larry Thibos [d], Steven K. Shevell [a,b,*]

[a] Psychology, University of Chicago, 940 E. 57th Street, Chicago, IL 60637, USA
[b] Ophthalmology & Visual Science and Institute for Mind & Biology, University of Chicago, 940 E. 57th Street, Chicago, IL 60637, USA
[c] Ecole Polytechnique de l'Université de Nantes, IRCCyN, Rue Ch. Pauc, La Chantrerie, BP 50609, 44306 Nantes Cedex 03, France
[d] School of Optometry, Indiana University, 800 E. Atwater Avenue, Bloomington, IN 47405, USA

ARTICLE INFO

Article history:
Received 23 May 2011
Received in revised form 11 August 2011
Available online 31 August 2011

Keywords:
Chromatic aberration
Wave aberrations
Optics
Retinal image
Spread light
Point spread function

ABSTRACT

The first physiological process influencing visual perception is the optics of the eye. The retinal image is affected by diffraction at the pupil and several kinds of optical imperfections. A model of the eye (Thibos & Bradley, 1999), which takes account of pupil aperture, chromatic aberration and wavefront aberrations, was used to determine wavelength-dependent point-spread functions, which can be convolved with any stimulus specified by its spectral distribution of light at each point. The resulting retinal spectral distribution of light was used to determine the spatial distribution of stimulation for each cone type (S, M and L). In addition, individual differences in retinal-image quality were assessed using a statistical model (Thibos, Bradley, & Hong, 2002) for population values of Zernike coefficients, which characterize imperfections of the eye's optics. The median and relatively extreme (5th and 95th percentile) modulation transfer functions (MTFs) for the S, M and L cones were determined for equal-energy-spectrum (EES) 'white' light. The typical MTF for S cones was more similar to the MTF for L and M cones after taking wavefront aberrations into account but even with aberrations the S-cone MTF typically was below the M- or L-cone MTF by a factor of at least 10 (one log unit). More generally, the model presented here provides a technique for estimating retinal image quality for the S, M and L cones for any stimulus presented to the eye. The model is applied to some informative examples.

1. Introduction

A single point of monochromatic light that enters the eye has a two-dimensional retinal image due to diffraction and imperfections of the eye's optics. The retinal image can be characterized by a point spread function (PSF), which varies with the wavelength of light. With broadband light, the retinal image is determined by decomposing the point of light into its spectral components; the PSF is applied separately at each wavelength (Barnden, 1974; Ravikumar, Thibos, & Bradley, 2008). The distribution of light on the retina is the superposition of the light distributions for each of the wavelengths. When an observer views a complete scene rather than a single point, each point in the scene is independently affected by the eye's optics; conceptually, the resulting retinal image at each wavelength is the superposition of the distribution of light from each point in the scene. Retinal image quality depends on both the PSF for each wavelength and the spatial and spectral distribution of the light in view.

Optical models of the eye have been sought for centuries for a variety of applications (Emsley, 1952; Smith, 1995). A relatively recent model (Thibos & Bradley, 1999) was used here to determine the spatial and spectral distribution of light on the retina; this distribution then was used to find the spatial distribution of light for each receptoral cone class, L, M and S. This model has two advantages in comparison to Marimont and Wandell's (1994) well known model of retinal image quality. First, higher-order wavefront aberrations were considered explicitly here rather than as an implicit property of a wavelength-independent point spread function (Marimont & Wandell, 1994, p. 3116). Second, the Thibos and Bradley model-eye depends on specific parameters (Zernike coefficients) that characterize an individual eye, and these parameters have a known multivariate population distribution. The population distribution allowed estimates of individual differences in retinal image quality among people with normal corrected vision (Thibos, Bradley, & Hong, 2002). While a general comparison of the retinal image quality given by the Marimont and Wandell model versus the one used here is not possible because the models depend on different assumptions, results from the two models are compared in Section 5 using a typical eye from the population distribution given by Thibos, Bradley, and Hong (2002). The two models agree well in this special case (as discussed later).

* Corresponding author at: Institute for Mind & Biology, University of Chicago, 940 E. 57th Street, Chicago, IL 60637, USA.
E-mail address: shevell@uchicago.edu (S.K. Shevell).

0042-6989/$ - see front matter © 2011 Elsevier Ltd. All rights reserved.
doi:10.1016/j.visres.2011.08.020

The first part of this paper focuses on retinal image formation. The optical model is described and the calculated photoreceptor absorptions are explained. In the second part, the model is applied to broadband 'white' spectral stimuli to assess typical and extreme retinal contrast sensitivity in a normal population of human observers. The third part considers some specific cases to show how retinal image quality depends on particular features of a visual stimulus, and to demonstrate how the model may be applied to particular types of images.

2. Part 1: Retinal image model

The retinal image is determined by characterizing the eye's optics. Any optical system can be fully described mathematically over an isoplanatic area by its optical transfer function (Williams & Becklund, 1989) so calculating the retinal image involves determining the eye's optical transfer function (OTF) or the closely related point spread function (PSF). The PSF gives the retinal image of a monochromatic point source, taking account of the optics of the eye. The OTF is the Fourier transform of the intensity PSF.

A precise model of the eye includes various optical factors that affect the PSF at each wavelength. This section covers the main properties of the model eye used to determine the PSFs. Recall that the external stimulus pattern entering the eye is decomposed into multiple monochromatic stimulus patterns, and then the stimulus pattern at each wavelength is convolved with its wavelength-dependent PSF. This gives the retinal image $I(x,y,\lambda)$ at each wavelength λ. Superposition of these monochromatic retinal patterns yields the retinal spectral distribution of light for each spatial location (x,y). These spectral distributions allow calculation of the spatial distribution $I_C(x,y)$ of cone excitation for each cone type C (C = L, M or S) by applying the appropriate cone spectral sensitivity function $S_C(\lambda)$ as a weighting factor:

$$I_C(x,y) = \int S_C(\lambda) I(x,y,\lambda) d\lambda. \quad (1)$$

2.1. Optics of the human eye

The human eye has three main optical components that affect retinal image quality: the pupil, the cornea and the lens. The pupil diffracts light entering the eye, resulting in a PSF with a central point surrounded by concentric rings (Roorda, 2002; Williams & Hofer, 2004). The cornea accounts for most of the eye's refraction (about 43 diopters) while the lens, which refracts light after passing through the pupil, adds more than 20 diopters in a young adult (Roorda, 2002). The cornea and lens are the primary contributors to wave aberrations, which degrade retinal image quality. In the study here, all of these factors were combined into a reduced-eye optical model containing a pupil and a single refracting surface that is distorted from an optically perfect ellipse to exactly mimic the monochromatic aberrations of the whole eye (Ravikumar, Thibos, & Bradley, 2008). To account for individual variation, numerous such models were constructed using a statistical distribution of aberrations in a normal population of healthy adult eyes, as elaborated below. The monochromatic imaging capability of each model eye is summarized by its PSF.

Longitudinal chromatic aberration (LCA) is a consequence of refraction by a dispersive medium: light of different wavelengths is brought into focus at different distances. The focal distance increases with wavelength. LCA was included in the model by allowing the Zernike coefficient C_2^0 for defocus to vary with wavelength as prescribed by the Indiana Eye model of chromatic aberration (Thibos, Ye, Zhang, & Bradley, 1992). Transverse chromatic aberration was ignored because of its weak marginal influence on image quality when LCA and wave aberrations are considered (Ravikumar, Thibos, & Bradley, 2008). Similarly, the slight effect of higher-order chromatic aberrations on image quality was not included (Nam, Rubinstein, & Thibos, 2010).

Retinal image quality depends on pupil size and the wavelength of light. The greatest loss of image quality from diffraction occurs with a small pupil and long wavelengths. On the other hand, the greatest loss from refractive elements occurs with a large pupil and short wavelengths. The sharpest retinal image, therefore, typically is at an intermediate pupil size near 3 mm, which balances the tradeoff between diffraction (worse at smaller pupil diameters) and the deleterious effects of wave aberrations (worse at larger diameters).

The best known wave aberrations caused by the eye's optics are defocus and astigmatism, which are ameliorated by standard corrective lenses. Higher-order wave aberrations (trefoil, coma, spherical, as well as other still higher-order aberrations) also reduce image quality (Packer & Williams, 2003). The imperfections captured by the higher-order wave aberrations include the irregularities in optical elements within the eye. The eye's lower- and higher-order wave aberrations can be modeled accurately using Zernike polynomials; the first 15 Zernike mode numbers were used here for the polynomials (Thibos & Bradley, 1999; Thibos, Hong, Bradley, & Cheng, 2002). Statistical sampling of Zernike aberration coefficients produced a random sample of 100 model eyes for analysis, each of which yielded monochromatic PSFs that were representative of human eyes (Thibos, 2009).

As mentioned above, each wavelength of light is affected differently by the optics of the eye so each wavelength has its own distinct PSF; we refer to the set of PSFs for all wavelengths in the visible spectrum as a hyperspectral PSF. Spectral sampling here was every 10 nm, a choice supported by the analysis of Ravikumar, Thibos, and Bradley (2008). A hyperspectral PSF captures two important aspects of retinal image quality. First, an object with a single broadband chromaticity, such as equal-energy-spectrum 'white', does not necessarily produce on the retina an image at only that chromaticity because some wavelengths are more strongly dispersed than others. Second, spectral mixtures that are visually indistinguishable in color as large homogenous patches (color metamers) may not match at other spatial frequencies because the wavelengths composing each metamer are unequally affected by optics (Marimont & Wandell, 1994; Poirson & Wandell, 1993).

An implication of the second point is that the influence of optics on the retinal image can be determined only from the full spectral distribution of light entering the eye. In general, a trichromatic description of the light – for example CIE X,Y,Z tristimulus values or the excitations of the three types of cones – is not sufficient. While some special cases can reduce the computational burden of multiple convolutions (for example, spectral homogeneity where every point in the image emits the same relative radiance spectrum, or when the full spectral distribution is uniquely determined by the trichromatic specification; Barnden, 1974; Ravikumar, Thibos, & Bradley, 2008), these conditions rarely occur in the natural world.

2.2. Cone quantal absorptions

Transduction of light at the photoreceptors establishes the neural responses that mediate vision. There are three classes of cone photoreceptor, labeled S, M and L, with peak sensitivity in the short-, middle- or long-wave part of the visible spectrum, respectively. The response of each cone type depends on the rate of quantal absorption. The relative spectral sensitivity of each type of cone is known (Smith & Pokorny, 1975) so the rate of quantal absorption for S, M or L cones can be calculated directly from the spectral energy distribution of light at each point on the retina. (The spacing

between adjacent cones in the retinal mosaic is ignored here.) This gives the spatial distribution of stimulation for each cone type.

The retinal spatial distribution of excitation for each cone type, therefore, requires the full spectral distribution of light at each point within the viewed scene. This implies, for example, that a scene on a color display with each pixel specified by its R ('red'), G ('green') and B ('blue') components must be transformed into a pixel-by-pixel spectral energy distribution in order to determine the retinal image. For example equal-energy-spectrum (EES) 'white' light, which by definition has all wavelengths in the visible spectrum at the identical energy, should not be used to calculate the retinal image of the *metamer* to EES on a color display because the display's weighted sum of the R, G and B components has a different physical spectral composition than true EES with all wavelengths at the same energy (compare dashed and solid lines, Fig. 1). Instead, calibration of the display is required to transform trichromatic coordinates of the display to the full spectral distribution of light at each point of the stimulus. This transformation is specific to each individual display; it differs among displays of the same manufacturer and model, and even for the same display over time.

3. Part 2: Typical and population extremes of retinal image quality

3.1. Point spread functions

The effects of pupil size and wave aberrations on the shape of the PSF can be determined separately. The PSFs shown in Fig. 2 ignore wavefront aberrations; only diffraction and longitudinal chromatic aberration (LCA) are included in the three PSFs, shown for wavelengths 400, 550 and 700 nm and with a 6 mm diameter pupil.

Zernike polynomials are used to model wavefront aberrations. A study conducted on 200 normal eyes was the basis for prior development of a multivariate statistical model for the population distribution of Zernike coefficients up to the 36th Zernike mode number. Fig. 3 shows the first 15 mean Zernike coefficients for a pupil diameter of 3.0, 4.5 or 6.0 mm from the work of Thibos, Bradley, and Hong (2002; some values in the figure were determined in that study though not explicitly presented in the paper). These results are consistent with other population studies (Castejon-Mochon, Lopez-Gil, Benito, & Artal, 2002; Porter, Guirao, Cox, & Williams, 2001; Salmon & van de Pol, 2006). In general, values of the Zernike coefficients vary with both the characteristics of a particular eye and with pupil size. As mentioned above, the slight variation expected in higher-order aberrations with wavelength

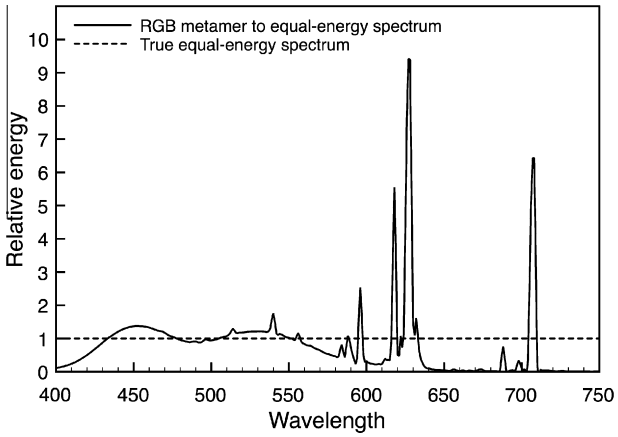

Fig. 1. Spectral power distribution of a true equal-energy-spectrum 'white' stimulus (dashed line) and from a typical color monitor displaying a light metameric to the equal-energy spectrum (solid line).

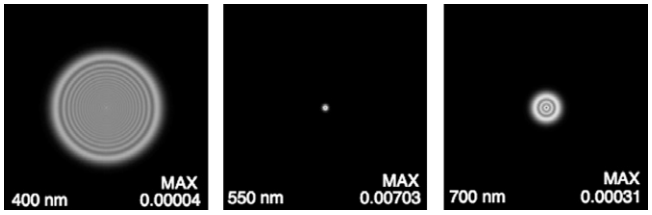

Fig. 2. Point spread functions due to only diffraction and longitudinal chromatic aberration (no wavefront aberrations) for monochromatic wavelengths 400, 550 and 700 nm. Focus wavelength is 570 nm; 6 mm diameter pupil. The height and width of each panel is 1° of visual angle. The sum of the volume under the PSF in each panel is 1.0 but, for visual clarity, the maximum in each plot is scaled to appear white; the actual maximum in each plot, which varies by more than 175:1, is shown in the bottom right of each panel.

and the variation of the prismatic terms responsible for transverse chromatic aberration were ignored (Nam, Rubinstein, & Thibos, 2010).

Point spread functions that include wave aberrations are shown in Fig. 4 for a 6 mm diameter pupil, which is close to the pupil size for 20–30 year-old observers at a luminance of about 100 cd/m^2 (Winn, Whitaker, Elliott, & Phillips, 1994). Analyses that follow also use a 6 mm diameter pupil. The mean Zernike coefficients from Fig. 3c were used for the PSFs in Fig. 4a but, as discussed below, these PSFs are not characteristic of a typical human eye. The PSFs in Fig. 4b are based on Zernike coefficients for a "standard observer" described later.

3.2. Modulation transfer functions and phase shifts

The modulation transfer function (MTF) is used to assess the eye's optical quality. Conceptually, the MTF can be determined for an EES light or any other spectral distribution by finding the contrast in the retinal image for sine waves at various spatial frequencies.

L-, M- and S-cone MTFs were determined here for 100 different independent random samples of Zernike coefficients taken from the population distribution given by Thibos, Bradley, and Hong (2002). The first 15 Zernike coefficients were used. The spectral distribution of light was EES, and luminance was varied sinusoidally in the horizontal direction (i.e., a vertically oriented sine wave). The wavelength in focus was fixed at 570 nm, which is the average wavelength that is optimally focused when observers report that white-light targets are best focused (Coe, 2009). With the PSFs determined for each visible wavelength, the retinal image at each wavelength was found by convolving the PSF for that wavelength with the visual stimulation at that wavelength. Repeating this for each wavelength in the stimulus and then taking the superposition of all wavelengths gave the spectral distribution of light at each point on the retina resulting from a particular visual stimulus (for example, an EES sine-wave grating varied in luminance at 10 cycles per degree). Then, at each point on the retina, the amount of each wavelength was weighted by the Smith and Pokorny (1975) cone spectral sensitivity function, separately for the L, M and S cones. This gave the relative quantal absorption for each cone type at that point on the retina. The MTF for each cone type then was determined by finding the retinal contrast as a function of the spatial frequency of the stimulus.

The complete set of one hundred MTFs, determined separately for the L, M, and S cones, is shown in Fig. 5 (thin gray lines). The median (thick black line), 5th percentile (dotted line) and 95th percentile (dashed line) values are also shown. The figure reveals the large individual differences in the MTFs estimated to occur within a normal population. The S-cone median MTF is well below the L- and M-cone median curves, though the population variation for each cone's MTF is large.

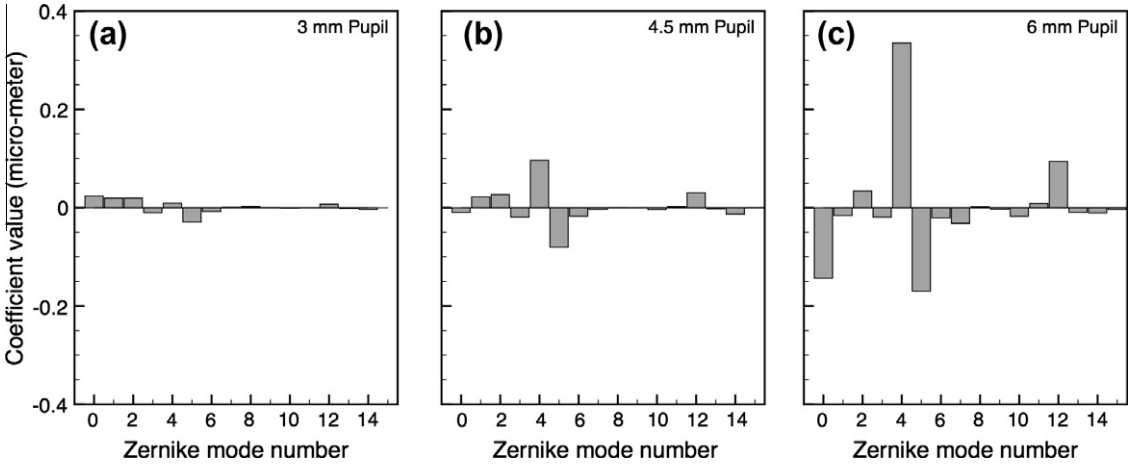

Fig. 3. Mean Zernike coefficients for the first 15 Zernike modes, for pupil diameter (a) 3 mm, (b) 4.5 mm or (c) 6 mm (from the model of Thibos, Bradley, & Hong, 2002).

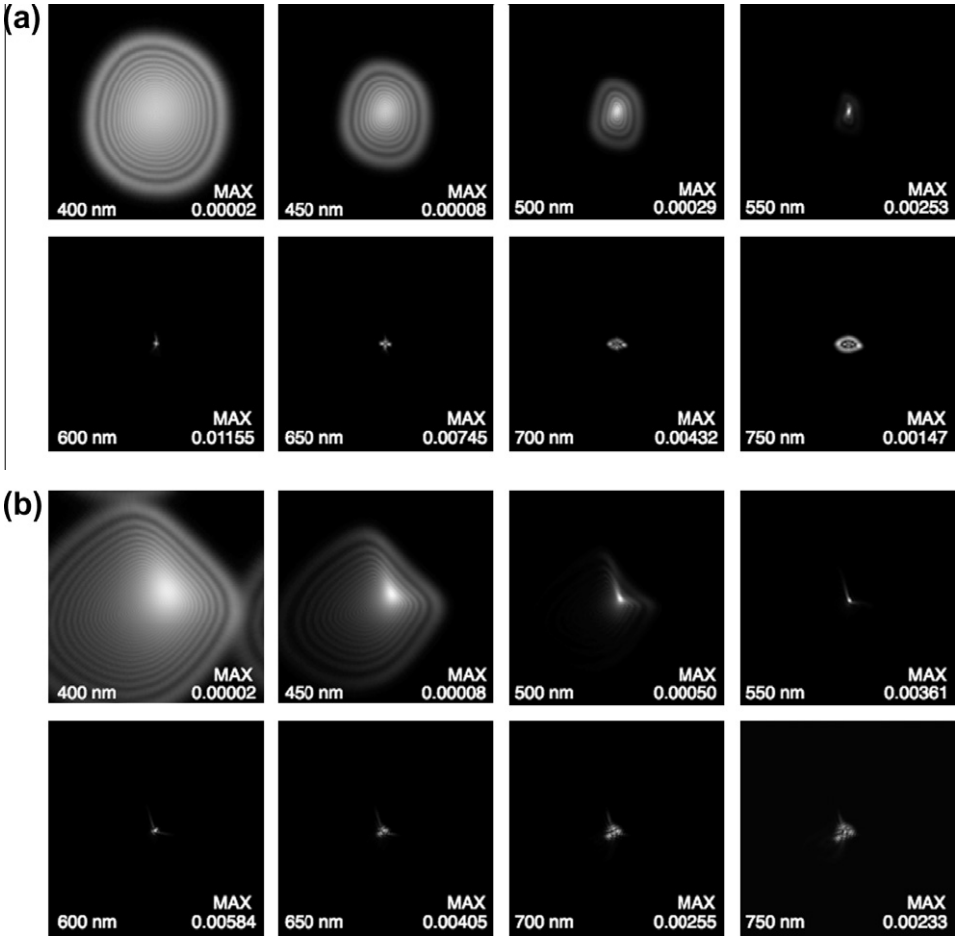

Fig. 4. As Fig. 2 but for point spread functions due to diffraction, longitudinal chromatic aberration, and wavefront aberrations, for monochromatic wavelengths 400, 450, 500, 550, 600, 650, 700 and 750 nm. The maximum of each plot is set to be white; the actual maximum, which varies by over 500:1, is shown in the bottom right of each panel. (a) Based on mean population Zernike coefficients from Fig. 3c. (b) Based on Zernike coefficients for a "standard observer" (see text and Table 1).

One sampled set of Zernike coefficients gave L-, M- and S-cone MTFs that were close to the median values (see lines connecting symbols, Fig. 5). This set of Zernike coefficients (Table 1) was used to define a "standard observer" for a 6 mm pupil; the MTFs from this set were consistent with an observer with about half the sample having better retinal cone contrast and half having worse contrast. While the standard observer's S-cone MTF is slightly better than the median (at worst the 65 percentile instead of the median's 50 percentile, at 10 cycles per degree), this set of sampled Zernike coefficients was selected for the standard observer because the set of coefficients gave values close to both the median MTFs (Fig. 5) and the median magnitudes of image displacement (computed as the ratio of absolute value of phase shift to spatial frequency), for all three types of cone. The absolute value of image displacements from the 100 random independent samples of Zernike coefficients is shown in Fig. 6. The median absolute values were close to the image

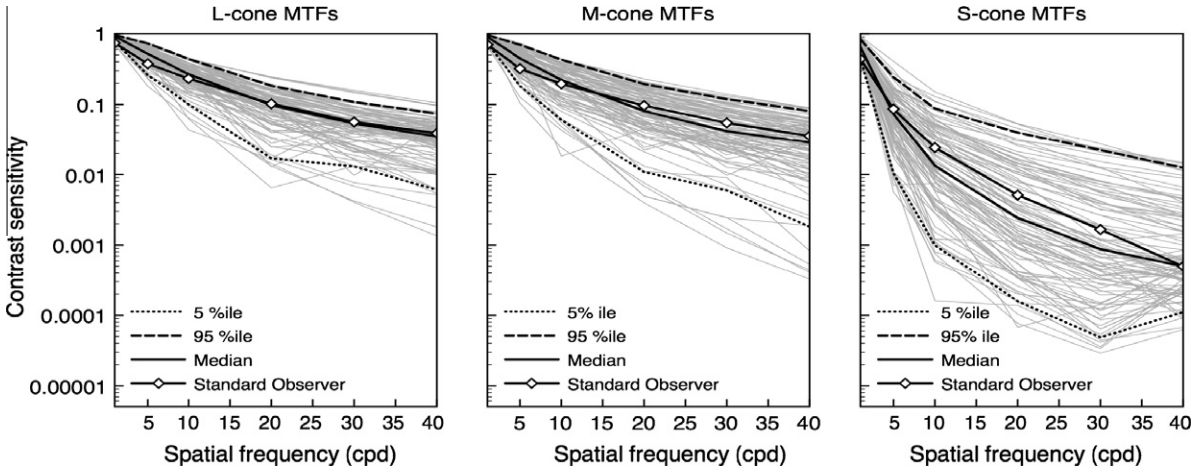

Fig. 5. Modulation transfer functions for 100 randomly sampled sets of Zernike coefficients for pupil diameter 6 mm (gray lines). The median contrast sensitivity among the 100 values at each spatial frequency is shown by the solid black line; the 5th and 95th percentile contrast sensitivity is shown by dotted and dashed lines, respectively. The solid black lines connecting the symbols are MTFs for the "standard observer" (see text). (Left) L-cone MTFs. (Middle) M-cone MTFs. (Right) S-cone MTFs.

Table 1
Zernike coefficients for "standard observer" with 6 mm pupil.

Zernike mode number	Coefficient value
0	0.3243
1	−0.5796
2	0.7083
3	−0.1115
4	0.8638
5	0.0148
6	−0.1116
7	−0.1644
8	0.3053
9	−0.0673
10	−0.0273
11	−0.0115
12	0.2394
13	0.0228
14	0.0784

displacements for the standard observer (compare solid lines, with and without symbols, Fig. 6). Of course, this particular set of Zernike coefficients is not unique in terms of giving MTFs and image displacements that are near the medians for all three cone types.

The significance of spatial phase shifts in the image plane should not be ignored when wave aberrations are introduced. A circularly symmetric PSF due only to diffraction and longitudinal chromatic aberration (i.e., no wave aberrations, as in Fig. 2) causes either a zero or 180° phase shift (i.e., phase reversal) in the stimulus. Wave aberrations, however, can shift phase in the image plane by arbitrary amounts. A PSF reflects both the MTF and phase shifts so a full description of the retinal image requires an accurate representation of both. While several other sampled sets of Zernike coefficients gave MTFs close to the median for the three cone types (Fig. 5), the standard observer was selected to closely represent both the median MTFs (Fig. 5) and median image displacements (Fig. 6).

Note the larger image displacements for S than for M and L cones in the population, for both the median and extreme (95th percentile) values (Fig. 6).

To assess the reliability of the median and extreme MTFs, the 100 sampled sets of Zernike coefficients were randomly split into two groups of 50 samples each. Then the median, 5th percentile and 95th percentile MTFs for the L-, M- and S-cone were compared for the two halves. The comparison of the two groups showed good agreement (Fig. 7).

A straightforward way to quantify the differences in MTFs among the L, M and S cones is to plot relative M/L and S/L contrast sensitivity for the median, 5th percentile and 95th percentile MTFs (Fig. 8). This shows that median contrast sensitivity is similar for the M and L cones. Median S-cone contrast sensitivity is a log unit or more lower than L, except at the lowest spatial frequencies.

3.3. Zernike coefficients: population means versus values for standard observer

There are substantial differences between the Zernike coefficients for the "standard observer" (Table 1, and gray bars in Fig. 9) and the mean Zernike coefficients for the population of human observers (diamonds, Fig. 9; replotted from Fig. 3c). For most purposes, calculations based on Zernike-coefficient population means are not representative of a typical observer's image quality (Thibos et al., 2002). A way to visualize the significance of the difference between the two sets of Zernike coefficients is to compare the wavelength-dependent PSFs based on population-mean coefficients with the PSFs for the "standard observer" (Fig. 4a and b, respectively). The PSFs for the standard observer are less circularly symmetric, as expected for Zernike coefficients that are farther from zero.

Even more significant is the difference in the MTFs based on mean Zernike coefficients versus the Zernike coefficients for the standard observer. Consider again the median, 5th percentile and 95th percentile MTFs for the 100 randomly sampled sets of Zernike coefficients for pupil diameter 6 mm (Fig. 10, replotted from Fig. 5), and compare them to (i) MTFs for the standard observer and (ii) MTFs implied by the mean Zernike coefficients (open and solid symbols, respectively, in Fig. 10). The MTFs for the standard observer fall close to the medians, of course, because of the criteria used to define the standard observer. The L- and M-cone MTFs based on population-mean Zernike coefficients are near or above the 95th percentile MTFs; they show that mean Zernike coefficients give estimates of image quality appropriate for only a very small fraction of the population with the best optics.

4. Part 3: Estimating specific retinal images: issues and examples

The first two parts of the paper considered retinal image quality and how it affects stimulation of the L, M and S cones for typical

and relatively extreme normal human observers, assuming a 'white' stimulus with an EES spectral distribution. MTFs were derived using vertical sine-wave gratings. More generally, the model developed above may be applied to any visual stimulus. In this part, retinal image quality is determined for other types of stimuli, with a focus on some informative cases.

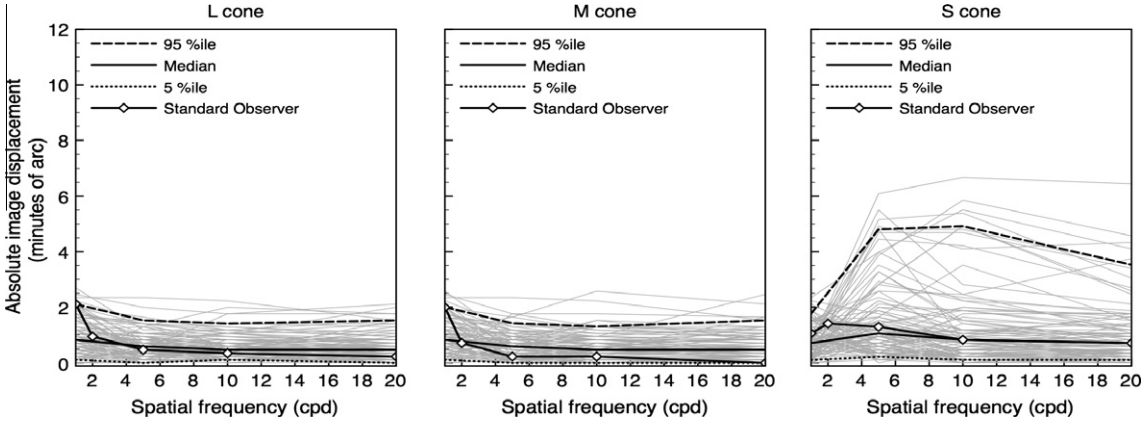

Fig. 6. Image displacement functions for 100 randomly sampled sets of Zernike coefficients (6 mm diameter pupil). Ordinate values are the ratio of |phase shift|/spatial frequency. The median, 5th percentile and 95th percentile shifts are indicated by solid, dotted and dashed black lines, respectively. Solid black lines connecting the symbols are image displacements for the standard observer whose Zernike coefficients are given in Table 1. (Left) L cone. (Middle) M cone. (Right) S cone.

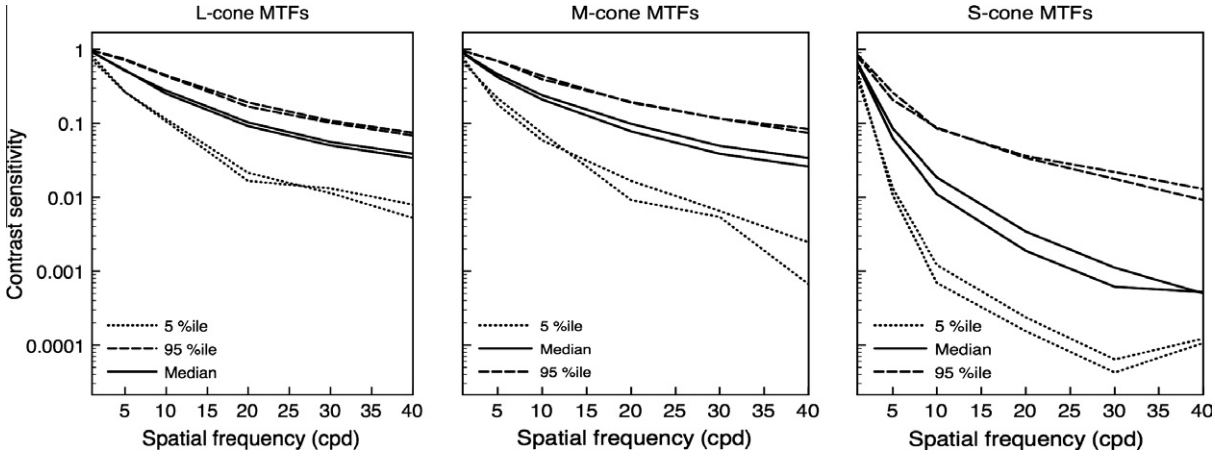

Fig. 7. Modulation transfer functions for split halves of the 100 randomly sampled sets of Zernike coefficients for pupil diameter 6 mm. Each split half had 50 sampled sets of Zernike coefficients. The median, 5th percentile and 95th percentile contrast sensitivity for each split half are shown as a function of spatial frequency by the solid, dotted and dashed lines, respectively. (Left) L-cone MTFs. (Middle) M-cone MTFs. (Right) S-cone MTFs.

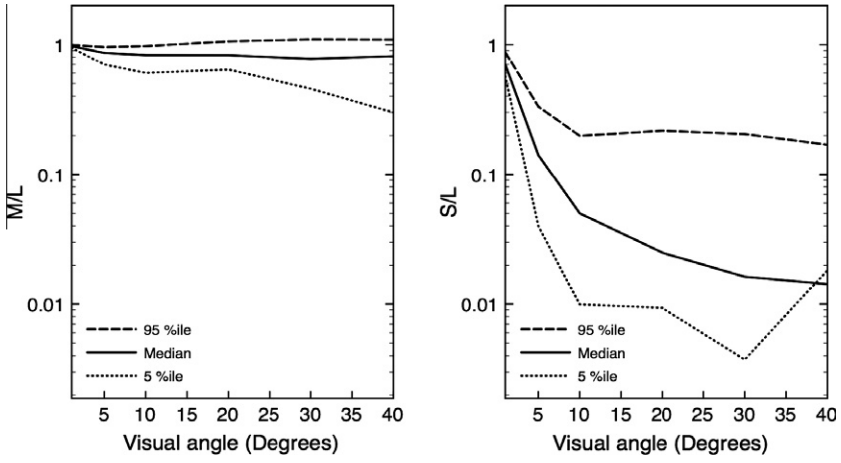

Fig. 8. The ratio of contrast sensitivity as a function of spatial frequency, based on 100 randomly sampled sets of Zernike coefficients, for (left) M cones relative to L cones and (right) S cones relative to L cones. The median, 5th percentile and 95th percentile are shown in each panel by the solid, dotted and dashed line, respectively. Pupil diameter is 6 mm.

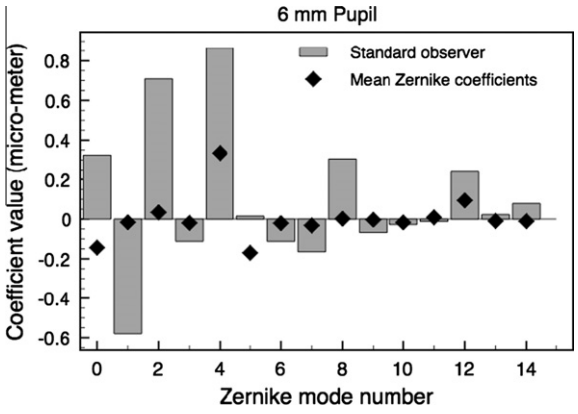

Fig. 9. The first 15 Zernike coefficients for the "standard observer" (6 mm diameter pupil, gray bars), whose MTFs and image displacements are similar to the median values from the 100 randomly sampled sets of Zernike coefficients. Mean Zernike coefficients are also shown (diamonds, replotted from Fig. 3c).

4.1. Equal-energy-spectrum 'white' and its CRT metamer

As discussed above, the eye's optical imperfections can be quantified by wavelength-dependent PSFs (Fig. 4), the effects of which are determined by decomposing the visual stimulus into its monochromatic components, applying each wavelength-dependent PSF, and then combining each monochromatic spatial light distribution by superposition. Thus, the effect of the eye's optics on the retinal spatial and spectral distribution of light depends on the spectral distribution of the stimulus.

The significance of the underlying spectral distribution of the stimulus can be missed by wrongly applying the color-vision principle of trichromacy, which holds that the color of any spectral distribution of light can be perfectly matched by a mixture of just three wavelengths (for example, 440 nm, 540 nm and 660 nm, which alone appear violet, yellowish-green and red, respectively). The basis for trichromacy is the three types of cone photoreceptors: L, M and S. Any given spectral distribution is perceived to be an exact match to an entirely different spectral distribution so long as both distributions have the identical rate of quantal absorption by the L, M and S cones; unequal spectral distributions that satisfy this matching criterion are called *metamers*. An example of two spectral distributions that appear identical is in Fig. 1. The flat energy distribution as a function of wavelength for EES 'white' (dashed line) results in the same stimulation of the L, M and S cones as the irregularly shaped spectral distribution (solid line), which is typical of a CRT display set to exactly match EES 'white'.

Two metameric spectral distributions of light, however, may not have exactly the same appearance when presented as complex patterns of light. The reason is that the underlying wavelength distributions that deliver identical rates of L-, M- and S-cone quantal absorptions for large uniform patches (as used for color matching) may be unequally affected by the eye's optics, because the effects of optics vary according to the wavelengths composing the two stimuli. For example, MTFs for the L and M cones for the standard observer are similar for true EES light and for its CRT metamer but contrast sensitivity for S cones is lower for true EES light compared to the metameric CRT chromaticity (compare open and filled symbols, Fig. 11). In general, retinal images of stimulus patterns composed of metameric lights may not be assumed to be equal.

4.2. Asymmetric retinal-image distortion and stimulus orientation

In the second part of the paper, MTFs were determined from luminance modulation of EES light varied in the horizontal direction (i.e., vertically oriented gratings). In the absence of wave aberrations, any orientation of the stimulus gives the same results because PSFs are circular (Fig. 2). PSFs that include effects of wave aberrations, however, are not circular in shape (Fig. 4) so the retinal image of even a uniform bar of light can (i) be asymmetric with respect to the center of the uniform bar and (ii) depend on stimulus orientation.

Asymmetric distortion from wave aberrations can be illustrated with a square-wave EES grating of two cycles per degree with 100% luminance contrast (solid lines, Fig. 12); in the figure, the one-dimensional square-wave is a profile of a two-dimensional vertical square-wave grating. Retinal-image profiles at monochromatic wavelengths between 400 and 750 nm are shown for a 6 mm pupil (Fig. 12). In the top panel, only diffraction and LCA are considered (no wave aberrations). The wavelength-dependent distortion of the square-wave stimulus is symmetric around the center of the stimulus peaks and troughs. By comparison, when wave aberrations for the standard observer are included (middle panel, Fig. 12), there is clear left–right asymmetry; moreover, the shape of the asymmetry is wavelength dependent. The asymmetry carries over to the spatial profile of stimulation for the L, M and S cones (bottom panel, Fig. 12).

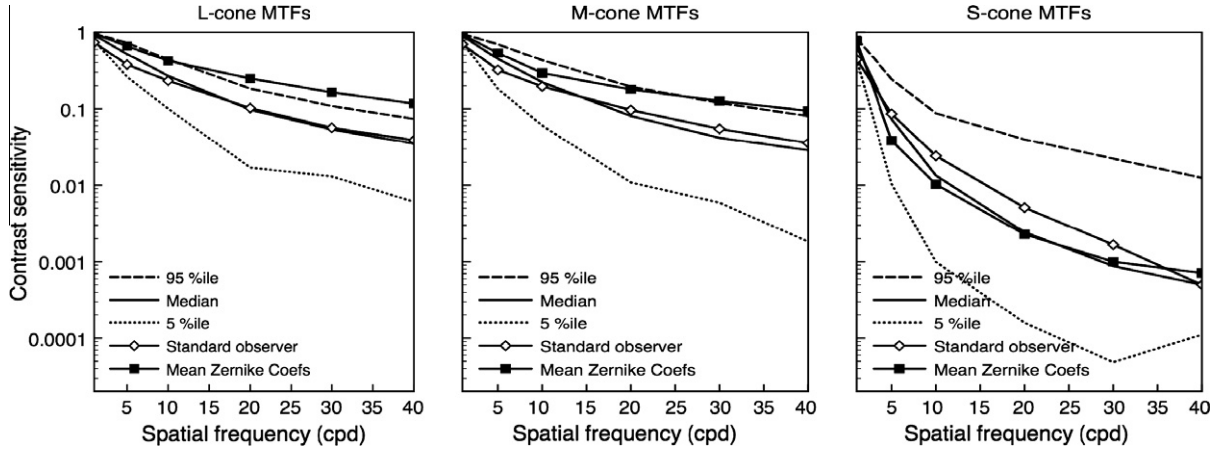

Fig. 10. Median, 5th and 95th percentile modulation transfer functions based on 100 randomly sampled sets of Zernike coefficients for pupil diameter of 6 mm (replotted from Fig. 5), compared to MTFs for the "standard observer" (solid lines connecting open symbols) and to MTFs based on the mean Zernike coefficients in Fig. 3c (solid lines connecting solid symbols). (Left) L-cone MTFs. (Middle) M-cone MTFs. (Right) S-cone MTFs.

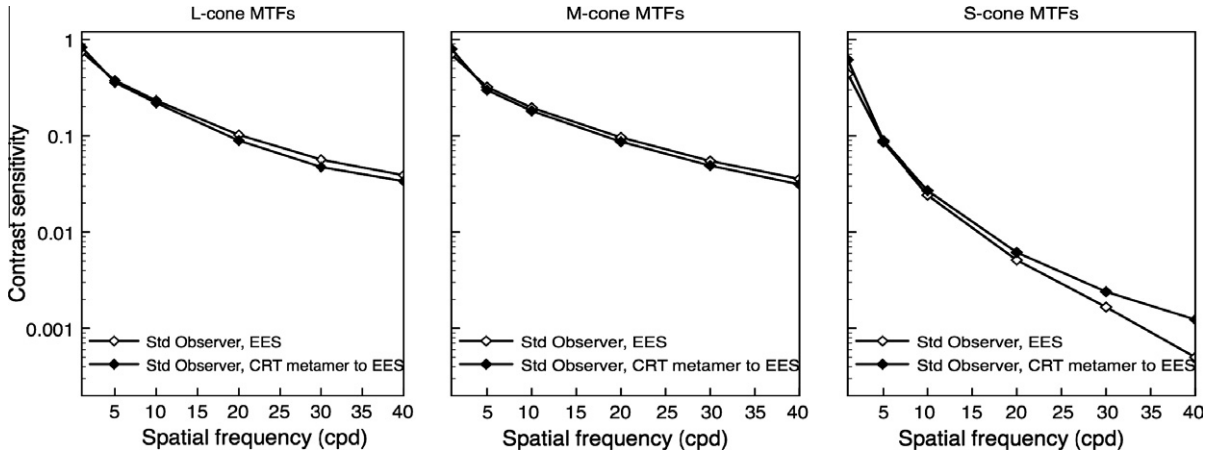

Fig. 11. Modulation transfer functions for the "standard observer" for vertical gratings composed of (i) EES 'white' light (open symbols) or (ii) the typical spectral distribution from a CRT display set to be metameric to EES 'white' (filled symbols). (Left) L-cone MTFs. (Middle) M-cone MTFs. (Right) S-cone MTFs.

The influence of stimulus orientation can be seen with the same EES, two cycle per degree square-wave grating. For the standard observer (6 mm pupil), the retinal-image profiles for the L, M and S cones are different for a vertically compared to horizontally oriented grating (see dotted and dashed lines, Fig. 13). In general, when wave aberrations are considered, the retinal image depends on the overall stimulus orientation as well as the spectral and spatial distribution of light.

4.3. The retinal image of an EES 'white' E

The loss in retinal image quality caused by the eye's optics can be visualized by the retinal image of the letter "E" of width 0.5° visual angle (cf. Williams & Hofer, 2004).

An E presented to the eye as EES 'white' light is shown in the far left panel of Fig. 14. The retinal image of the E, assuming only diffraction and LCA (no wave aberrations), is in the three top panels on the right, separately for stimulation of the L, M and S cones. A modest drop in image quality is apparent for the L-cone and M-cone retinal images, while the S-cone retinal image is far worse than for L or M. Adding wave aberrations of the standard observer (bottom three panels at right) further degrades the L-cone and M-cone retinal images but not the S-cone image, which actually appears a bit better than the S-cone image without wave aberrations. Note, however, that the S-cone retinal image with wave aberrations (bottom right panel) is poorer than the L- and M-cone images that include wave aberrations (compare three bottom panels at right, Fig. 14). The effect of wave aberrations on the retinal image for each type of cone is taken up again in Section 5, where previous studies are considered.

4.4. Retinal image quality for typical R, G and B components of a color video display

The model developed here may be applied to a visual stimulus with any spectral distribution. Three spectra of practical interest are the R, G and B components of a color video display. The analysis below is for the R, G and B guns of a Sony GDM-F520 CRT, a display used in many vision laboratories. (The exact R, G and B spectra vary, of course, from one video display to another.)

For any known spectral distribution of light, the MTF can be determined for the L, M or S cones of the standard observer. The R, G and B spectra of the CRT were measured using a PhotoResearch PR-650 spectroradiometer. For each type of cone (L, M or S), the R, G and B phosphor MTFs are plotted together in a single panel of Fig. 15. There are two main points. First, the MTFs for R and G are higher than for B, for every type of cone. Second, the MTFs for the R and G components are similar to each other for the L and M cones but not for the S cones, for which G has substantially higher contrast sensitivity than R. For S cones, in fact, contrast sensitivity for R is nearly as poor as for B.

5. Discussion

The approach here used a comprehensive model of the eye (Thibos & Bradley, 1999) that incorporates pupil aperture, longitudinal chromatic aberration and wavefront aberrations. The model gives the spatial and spectral distribution of light on the retina from any image presented to the eye. Such distributions were used to determine typical and extreme (5th and 95th percentile) MTFs for each type of cone (L, M and S), by incorporating known individual differences for the eye's optics (Thibos, Bradley, & Hong, 2002).

A large number of random samples from the statistical distribution for individual differences also revealed median levels of contrast sensitivity, from which a "standard observer" was defined with retinal image quality near the central tendency of the normal human population. Typical image quality is better represented by this standard observer than by calculations based on population-mean Zernike coefficients because mean values tend to cancel out positive and negative coefficients and thus underestimate the loss of image quality, which is largely dependent on the coefficients' magnitudes regardless of sign.

Other investigators have examined related questions about retinal image quality for spectrally broadband images. Results from the approach here are compared below to two well known studies.

5.1. A comparison to the Marimont and Wandell model

As mentioned in the Introduction, Marimont and Wandell (1994) consider a similar problem but with a model that has two important differences. First, the model here explicitly considers higher-order wavefront aberrations. Second, the model here can be used to estimate individual differences based on the statistical population distribution for characteristics of the eye's optics (Thibos, Bradley, & Hong, 2002). Nonetheless, in special cases the two models should give similar results. In particular, when only diffraction and longitudinal chromatic aberration are included in the model here (no wave aberrations), the modeled retinal image

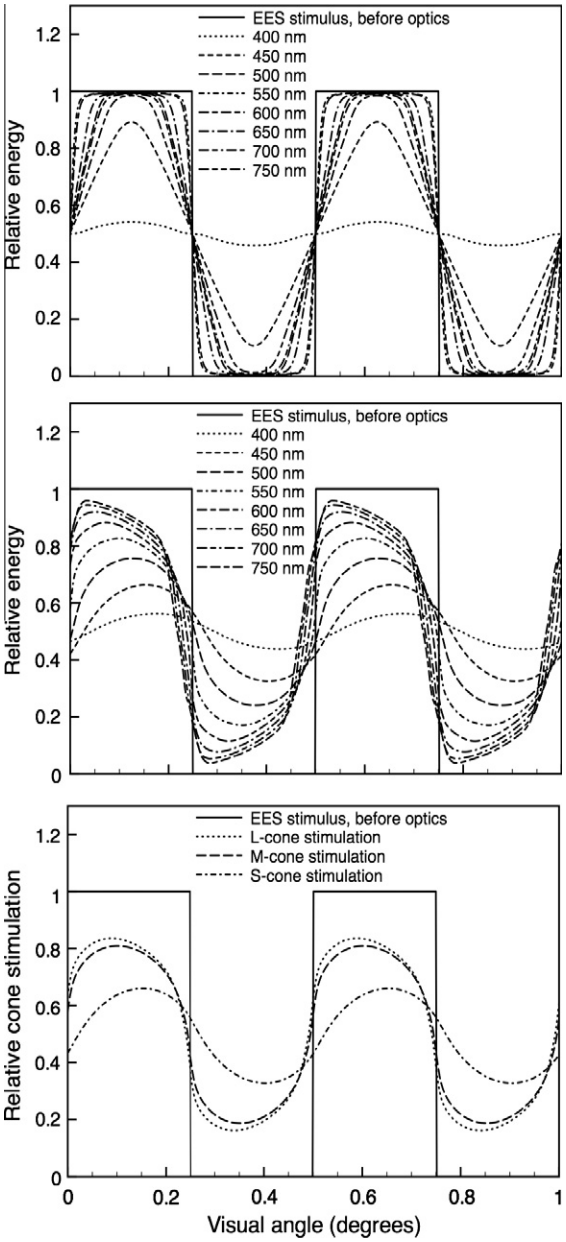

Fig. 12. Retinal-image profiles for an EES, two cycle per degree, 100% contrast square-wave grating. The solid line in each panel shows the square-wave stimulus. (Top and middle) Profiles for wavelengths 400, 450, 500, 550, 600, 650, 700 and 750 nm (6 mm pupil, 570 nm focus wavelength), with effects of only diffraction and longitudinal chromatic aberration (no wave aberrations, top) or with added effects of wave aberrations of the standard observer (middle). (Bottom) Retinal-image profiles for L-, M- and S-cone stimulation with wave aberrations of the standard observer.

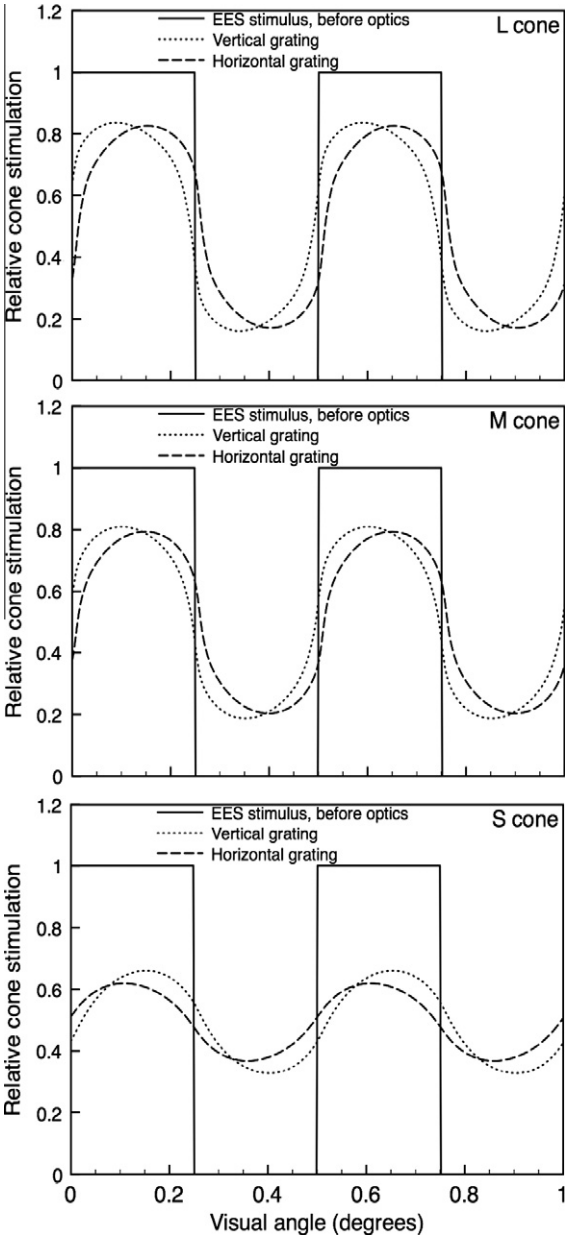

Fig. 13. Retinal-image profiles for an EES, two cycle per degree, 100% contrast square-wave grating (6 mm pupil, 570 nm focus wavelength) including effects of wave aberrations for the standard observer. The solid line in each panel shows the square-wave stimulus profile. The dotted and dashed lines show the profiles for a vertically or horizontally oriented grating, respectively. (Top) Relative L-cone stimulation; (Middle) relative M-cone stimulation; (Bottom) relative S-cone stimulation.

should be somewhat better than the results from the Marimont and Wandell model, which incorporates an approximation for higher-order aberrations. Also, the full model here with wave aberrations of the standard observer (Table 1) should give a retinal image similar to but different in shape than the Marimont and Wandell model, because introducing explicit wave aberrations results in asymmetries in the PSFs (Fig. 4) and thus in the retinal light profile (e.g., middle panel of Fig. 12).

Retinal light profiles for an inhomogeneous chromatic image (Fig. 16) were determined from the model here, both without and with wave aberrations (dotted and dash-dot lines, respectively), and from the Marimont and Wandell model (dashed line). For this test case, the stimulus was composed of a square-wave vertical stripe of width 7.3 min of arc, centered within a 1° wide surround. Both the stripe and surround had the same chromaticity (0.665) in the $l = L/(L + M)$ direction of the MacLeod and Boynton (1979) l,s cone-based coordinate system but differed in $s = S/(L + M)$: the stripe had an s chromaticity of 2.50 so when viewed alone would appear decidedly bluish, while the surround had an s chromaticity of 0.99 so was virtually metameric to EES 'white'. The stripe and surround were equal in luminance. The full spectral distributions of the chromaticities were assumed to be from the video display considered in Fig. 15.

In Fig. 16, the vertical axis is the light profile for the s chromaticity, derived from the retinal image for S, M and L and then applying the definition of $s = S/(L + M)$. The square wave (solid line) is

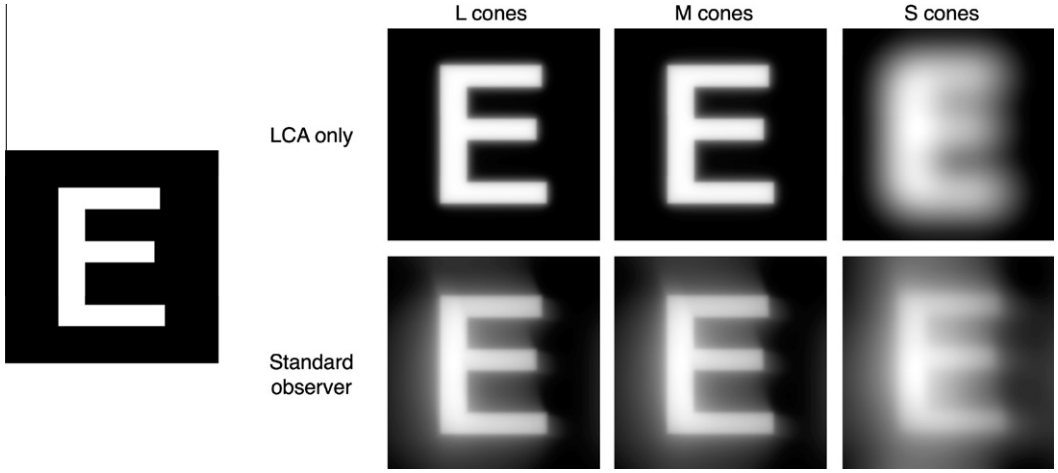

Fig. 14. Retinal images of an EES letter "E" subtending in width 0.5° visual angle. Each panel is 1° square and rendered relative to the maximum light level in the stimulus before entering the eye (shown at the far left). Pupil diameter is 6 mm. (Right, top row) The retinal image for the L, M and S cones assuming only diffraction and LCA (no wave aberrations). (Right, bottom row) The retinal image for the L, M and S cones with the added effects of wave aberrations of the standard observer.

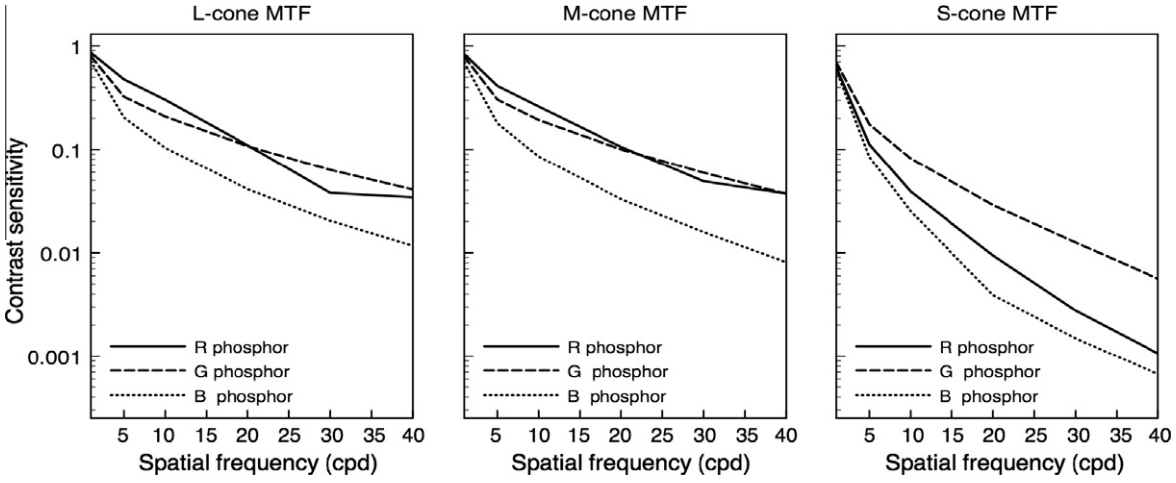

Fig. 15. Modulation transfer functions for the standard observer (6 mm diameter pupil) for vertical gratings composed of a typical video display's R phosphor, G phosphor or B phosphor. The MTFs for the L, M and S cones are shown separately in the left, middle and right panels, respectively. Focus wavelength 570 nm.

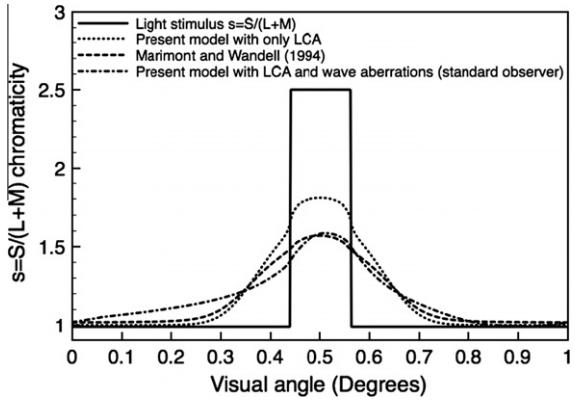

Fig. 16. Comparison between the retinal light profiles for $s = S/(L + M)$ from the model used here (focus wavelength 570 nm), without wave aberrations (dotted line) or with the wave aberrations of the standard observer (dash-dot line), and from the line spread function of Marimont and Wandell (dashed line). The corneal stimulus (solid line) is a vertical stripe of width 7.3 min within a 1° wide surround. The stripe and surround have different chromaticites (see text). Pupil diameter is 6 mm.

the image at the cornea. A technical point for calculation of s is selection of units for S, M and L; previous results for S-, M- and L-cone MTFs and light profiles were not dependent on units because plotted quantities were relative values. For Fig. 16, L and M were normalized so that L + M gave luminance (as for the Smith and Pokorny (1975) cone fundamentals), and S was scaled so that $s = 1.0$ for the spectrally flat distribution of EES 'white'.

As expected, the model here without wave aberrations specified a light profile for s that that was sharper (better retinal image quality) than either the Marimont and Wandell model or the model here that includes wave aberrations. The light profiles from the Marimot and Wandell model and from the model here with wave aberrations were similar but only the latter captured the asymmetry in the distribution of light implicit in the asymmetric PSFs (as seen in Fig. 4). Note that the light profile with higher-order wave aberrations (dash-dot line) depends on the orientation of the stripe in the stimulus. Overall, the comparison in this special case shows that the model used in this paper with the optics of the standard observer (Table 1) gives results in accord with those from the Marimont and Wandell model.

5.2. How do wave aberrations affect relative L-, M- and S-cone contrast sensitivity?

Longitudinal chromatic aberration (LCA) reduces the retinal image quality of broadband spectral light because the focal distance from refraction increases with wavelength. When light of some wavelength is in perfect focus, light at other wavelengths is blurred. MTFs that take account of both LCA and diffraction (but not wave aberrations) quantify the substantial reduction in retinal image quality that they cause for broadband EES 'white' light (left panel Fig. 17, lines without symbols).

Introducing wave aberrations also reduces image quality, compared to diffraction alone. The retinal image from diffraction, LCA and wave aberrations together – all of which, of course, affect natural viewing – might be expected to be worse than from only diffraction and LCA; somewhat surprisingly, however, adding the effects of wave aberrations to those of diffraction and LCA can improve image quality in some cases (McLellan, Marcos, Prieto, & Burns, 2002). The reason is that wave aberrations reduce the influence of wavelength on contrast sensitivity; although wave aberrations reduce contrast sensitivity at the wavelength of focus, they can increase sensitivity at other wavelengths that are badly defocused by LCA. The result is that wave aberrations in some cases "counteract retinal image blur from LCA (McLellan, Prieto, Marcos, & Burns, 2006, p. 3009)". For example, adding the standard observer's wave aberrations to diffraction and LCA reduces L- and M-cone contrast sensitivity but improves S-cone sensitivity (left panel Fig. 17, lines connecting symbols).

Comparing MTFs with versus without wave aberrations shows that introducing wave aberrations can make contrast sensitivity more similar for the three types of cone. For example at 20 cpd (see left panel, Fig. 17), with the wave aberrations of the standard observer the contrast sensitivity for L cones (and M cones) is about 20 times better than for S cones; without wave aberrations (only LCA and diffraction), L-cone (and M-cone) sensitivity is about 200 times better than S. These results confirm that wave aberrations can reduce the difference in contrast sensitivity among the three types of cone.

A related issue is whether wave aberrations fully (or nearly) eliminate the differences in contrast sensitivity for the L, M and S cones. McLellan et al. (2002) report that they do: the MTFs for all three cone types are nearly identical to each other, for each of their three observers (their Fig. 3b–d, p.175). To consider this question, the random sample of 100 sets of Zernike coefficients was searched for sets with the S-cone MTF near or above the L- and M-cone MTFs. For example, one sample (#14; middle panel, Fig. 17) had close L-, M- and S-cone MTFs (cf. the standard observer's MTFs in left panel of Fig. 17); the difference between L- and M-cone contrast sensitivity was about the same as between L and S sensitivity. At 20 cpd for #14, the contrast sensitivity for L cones was less than twice that of S cones. This set of MTFs is similar to the set for an observer reported by McLellan et al. (2002; their Fig. 3b). Another sample at 20 cpd (#92; right panel, Fig. 17) also had L-cone sensitivity less than two times higher than S, and at 40 cpd had S sensitivity fractionally better than L or M sensitivity (reminiscent of the MTFs for the observer in Fig. 3c of McLellan et al. (2002)). In sum, a few of the 100 samples were consistent with the view that wave aberrations can (nearly) eliminate contrast sensitivity differences among the three types of cone.

Recall, however, that the MTFs in the middle and right panels of Fig. 17 were selected from the sample of 100 sets because contrast sensitivity was similar for the L, M and S cones. To consider whether wave aberrations *typically* eliminate contrast-sensitivity differences among the three types of cone, the MTF for the S cones was compared to the MTFs for L and M cones at 10 and at 20 cpd for all 100 randomly sampled sets of Zernike coefficients. Because L- and M-cone MTFs tended to be similar, average L and M contrast sensitivity was compared to S sensitivity (that is, Average (L-sensitivity, M-sensitivity) relative to S-sensitivity). This sensitivity ratio for the 100 samples is plotted in a histogram in Fig. 18 (left panel, 10 cpd; right panel, 20 cpd). A value of zero indicates equal contrast sensitivity for S cones compared to the average for L and M; a positive [negative] value indicates L and M cones had higher [lower] sensitivity than S. The horizontal axis in Fig. 18 is a log scale so, for example, a value of +2.0 indicates lower S contrast sensitivity by a factor of 100.

Overall, S-cone contrast sensitivity nearly always was lower than L and M sensitivity (in 99% of cases at 10 cpd, and 97% of cases at 20 cpd). In the vast majority of cases, S contrast sensitivity was at least 10 times lower (>+1.0 on the log scale) than L and M sensitivity (73% of cases at 10 cpd, 77% of cases at 20 cpd). While S-cone sensitivity that is lower by a factor of 10 is a much smaller sensitivity difference than a factor of more than 200 for retinal image quality based on only diffraction and LCA (see arrows, Fig. 18), the results show that wave aberrations very seldom bring L-, M- and S-cone contrast sensitivity to comparable levels. The simulated

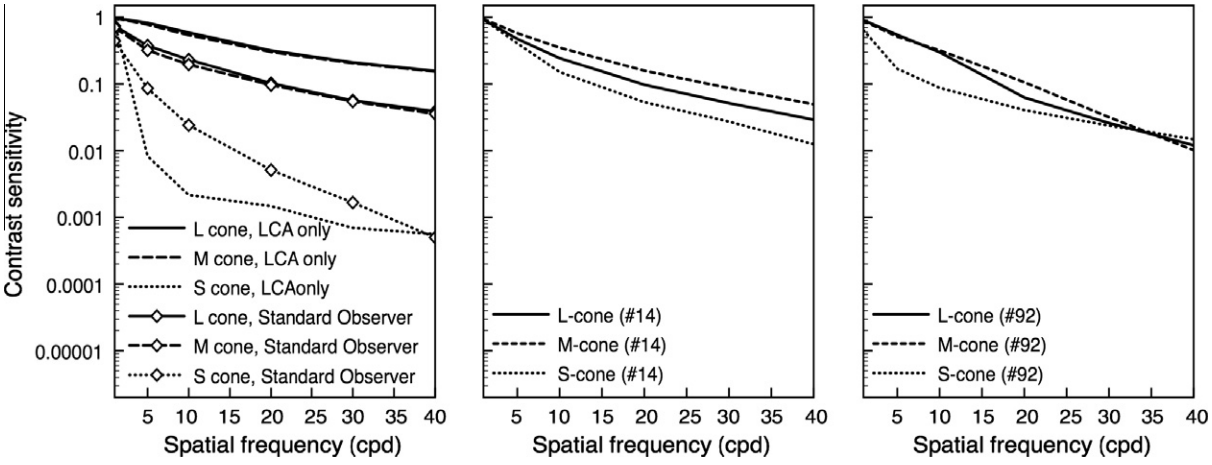

Fig. 17. (Left) The MTFs for each type of cone (L, M and S) with only diffraction and LCA (no wave aberrations, lines without symbols) and with the added wave aberrations of the standard observer (lines with symbols). (Middle and right) The L-, M- and S-cone MTFs for two (#14 and #92) of the 100 randomly sampled sets of Zernike coefficients, for which MTFs with wave aberrations were unusually similar for all three types of cone. For all panels, the spectral light distribution is EES, pupil diameter is 6 mm and focus wavelength is 570 nm.

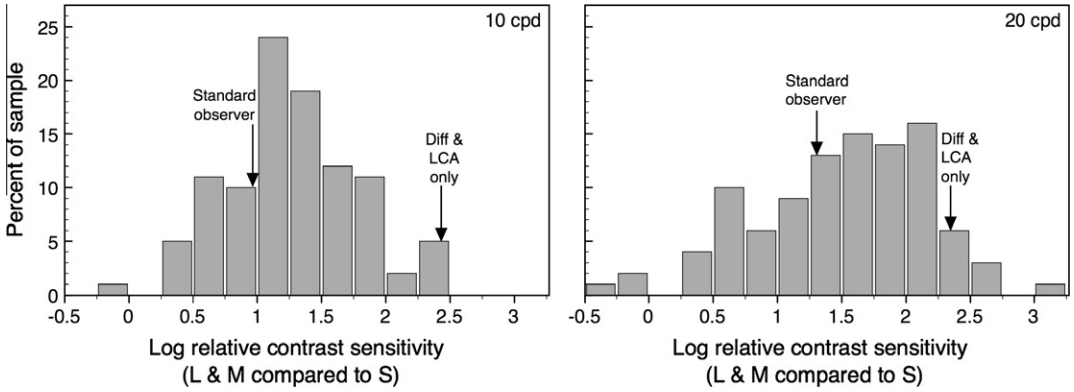

Fig. 18. Histogram of the contrast sensitivity ratio for the average for L and M cones compared to S cones, for the 100 randomly sampled sets of Zernike coefficients. Note the log scale on the horizontal axis. A positive value indicates lower S than L and M sensitivity. Pupil diameter is 6 mm and focus wavelength is 570 nm. (Left) 10 cpd. The value for the standard observer is 0.98, and for only diffraction and LCA (no wave aberrations) is 2.43. (Right) 20 cpd. The value for the standard observer is 1.30, and for only diffraction and LCA (no wave aberrations) is 2.33.

retinal image of the letter E (Fig. 14) is a demonstration of this point for the standard observer. The top three panels on the right of that figure include only diffraction and LCA; the image for S cones is far worse than for L and M. Wave aberrations, included in the images in the three bottom panels, further degrade the image for L and M cones but improve somewhat the image for S cones; nonetheless, even with wave aberrations the retinal image for S cones does not approach the quality of the image for L or M cones.

5.3. Other applications for the model of retinal image quality

The model used here can be employed for many other purposes. Psychophysical experiments aiming to infer neural processes often depend on knowledge of an accurate retinal (not corneal) spatial distribution of light. The model can be used to determine a typical retinal image for the standard observer, given any external stimulus; moreover, a population range of retinal images can be estimated for, say, the central 90% of the population by finding the extreme L-, M- and S-cone MTFs for the best and worst 5% of the population. This can be useful for excluding optical stimulus distortion as a viable account for experimental measurements, thereby implicating neural processes.

The pupil is largest, and retinal image quality often poorest, with dim illumination. A straightforward generalization of the model is to substitute the scotopic luminosity function $V'(\lambda)$ for the cone spectral sensitivity function $S_C(\lambda)$ in Eq. (1). This gives the spatial distribution $I_R(x,y)$ for rod excitation, from which a rod MTF or other characteristics of rod stimulation can be determined.

The model's capability to incorporate population variation in retinal image quality can be applied to several practical issues, including design decisions for instruments, spectral illumination and chromatically complex surfaces. An estimate of the retinal image for any light stimulus, including any object under any illuminant, can be useful for example to determine the legibility of text for, say, 99% of the population by assuming retinal image quality for the worst 1% of normal human observers. This may be particularly valuable for examining nighttime visibility (for example, for signage), when the pupil is largest. More generally, standards can be developed for detection or discrimination that take account of losses in retinal image quality for the vast majority of the normal population (say 99%, again by using retinal image quality for the worst 1% of the normal population). A related application is assessment of image quality (digital or otherwise). The ability to incorporate normal variation in the eye's optics permits perceived image-quality assessments to take account of the substantial variation in the retinal image, which depends on both the particular image presented to the eye and individual differences within the population of human observers.

Acknowledgment

Supported by NIH Grants RO1 EY-05109 (L.T.) and RO1 EY-04802 (S.S.).

References

Barnden, R. (1974). Calculation of axial polychromatic optical transfer function. *Optica Acta, 21*, 981–1003.
Castejon-Mochon, J. F., Lopez-Gil, N., Benito, A., & Artal, P. (2002). Ocular wave-front aberration statistics in a normal young population. *Vision Research, 42*, 1611–1617.
Coe, C. (2009). *Effect of monochromatic aberrations and wavelength on refraction and visual performance*. Doctoral dissertation, Indiana University (UMI Number: 3358910).
Emsley, H. H. (1952). *Visual optics* (5th ed.). London: Hatton Press.
MacLeod, D. I. A., & Boynton, R. M. (1979). Chromaticity diagram showing cone excitation by stimuli of equal luminance. *Journal of the Optical Society of America, 69*, 1183–1185.
Marimont, D. H., & Wandell, B. A. (1994). Matching color images: The effects of axial chromatic aberration. *Journal of the Optical Society of America A, 11*, 3113–3122.
McLellan, J. S., Marcos, S., Prieto, P. M., & Burns, S. A. (2002). Imperfect optics may be the eye's defence against chromatic blur. *Nature, 417*, 174–176.
McLellan, J. S., Prieto, P. M., Marcos, S., & Burns, S. A. (2006). Effects of interactions among wave aberrations on optical image quality. *Vision Research, 46*, 3009–3016.
Nam, J., Rubinstein, J., & Thibos, L. (2010). Wavelength adjustment using an eye model from aberrometry data. *Journal of the Optical Society of America A, 27*, 1561–1574.
Packer, O., & Williams, D. R. (2003). Light, the retinal image, and photoreceptors. In S. K. Shevell (Ed.), *The science of color* (2nd ed., pp. 41–102). Oxford: Elsevier.
Poirson, A. B., & Wandell, B. A. (1993). Appearance of colored patterns: Pattern-color separability. *Journal of the Optical Society of America A, 10*, 2458–2470.
Porter, J., Guirao, A., Cox, I. G., & Williams, D. R. (2001). Monochromatic aberrations of the human eye in a large population. *Journal of the Optical Society of America A, 18*, 1793–1803.
Ravikumar, S., Thibos, L. N., & Bradley, A. (2008). Calculation of retinal image quality for polychromatic light. *Journal of the Optical Society of America A, 25*, 2395–2407.
Roorda, A. (2002). Human visual system – Image formation. In J. P. Hornak (Ed.). *The encyclopedia of imaging science and technology* (Vol. 1, pp. 539–557). New York: John Wiley & Sons.
Salmon, T. O., & van de Pol, C. (2006). Normal-eye Zernike coefficients and root-mean-square wavefront errors. *Journal of Cataract and Refractive Surgery, 32*, 2064–2074.
Smith, G. (1995). Schematic eyes: History, description and applications. *Clinical and Experimental Optometry, 78*, 176–189.
Smith, V. C., & Pokorny, J. (1975). Spectral sensitivity of the foveal cone photopigments between 400 and 500 nm. *Vision Research, 15*, 161–171.

Thibos, L. N. (2009). Retinal image quality for virtual eyes generated by a statistical model of ocular wavefront aberrations. *Ophthalmic and Physiological Optics, 29*, 288–291.

Thibos, L. N., & Bradley, A. (1999). Modeling the refractive and neuro-sensor systems of the eye. In P. Mouroulis (Ed.), *Visual instrumentation: Optical design and engineering principles* (pp. 101–159). New York: McGraw-Hill.

Thibos, L. N., Bradley, A., & Hong, X. (2002). A statistical model of the aberration structure of normal, well-corrected eyes. *Ophthalmic and Physiological Optics, 22*, 427–433.

Thibos, L. N., Hong, X., Bradley, A., & Cheng, X. (2002). Statistical variation of aberration structure and image quality in a normal population of healthy eyes. *Journal of the Optical Society of America A, 19*, 2329–2348.

Thibos, L. N., Ye, M., Zhang, X., & Bradley, A. (1992). The chromatic eye: A new reduced-eye model of ocular chromatic aberration in humans. *Applied Optics, 31*, 3594–3600.

Williams, C. S., & Becklund, O. A. (1989). *Introduction to the optical transfer function*. New York: John Wiley & Sons.

Williams, D., & Hofer, H. (2004). Formation and acquisition of the retinal image. In L. M. Chalupa & J. S. Werner (Eds.). *The visual neurosciences* (Vol. 1, pp. 795–810). Cambridge, MA: MIT Press.

Winn, B., Whitaker, D., Elliott, D. B., & Phillips, N. J. (1994). Factors affecting light-adapted pupil size in normal human subjects. *Investigative Ophthalmology & Visual Science, 35*, 1132–1137.